Magazine of Concrete Research
Volume 66 Issue 18

Effect of multi-walled carbon nanotubes on mechanical properties of high-performance mortar
Sahranavard, Haji-Kazemi and Abbasi

Magazine of Concrete Research, 2014, **66**(18), 948–954
http://dx.doi.org/10.1680/macr.14.00037
Paper 1400037
Received 29/01/2014; revised 10/04/2014; accepted 15/04/2014
Published online ahead of print 24/07/2014

ice
Institution of Civil Engineers
publishing

Effect of multi-walled carbon nanotubes on mechanical properties of high-performance mortar

Saeed Sahranavard
MEng Student, Department of Civil Engineering, Ferdowsi University of Mashhad, Mashhad, Iran

Hasan Haji-Kazemi
Professor, Department of Civil Engineering, Ferdowsi University of Mashhad, Mashhad, Iran

Sedighe Abbasi
PhD Student, Esfarayen University, Esfarayen, Iran

High-performance mortars (HPMs) are very compact handmade composites with high compressive strength and low permeability and flexibility. Because of these properties, HPMs are used in special structural and defensive structures. This paper reports on the influence of functionalised multi-walled carbon nanotubes (MWCNTs) on the impact resistance and compressive and flexural strengths of HPM. The functionalised MWCNTs were characterised using Fourier transform infrared (FTIR) spectroscopy and X-ray diffraction (XRD). FTIR analysis confirmed the presence of oxygen-containing groups such as hydroxyl and carboxyl on the surface of oxidised MWCNTs. The XRD results revealed a sharp peak at around $2\theta = 26°$ and a broad peak centred at $2\theta = 43°$, corresponding to the (002) and (100) Bragg reflection planes respectively. The results of tests on reinforced high-performance mortar containing 0·1 %wt MWCNTs show that the impact resistance, compressive strength and flexural strength were 1400%, 25·58% and 2% higher than those of HPM without MWCNTs. Furthermore, scanning electron microscopy test results show that the presence of MWCNTs has a significant effect on the microstructure of HPM.

Notation

b width of prismatic specimen
d depth of prismatic specimen
E unique impact energy
E_t energy of fracture
g gravitational acceleration
h falling height of sphere
L clear span of specimen in quasi-static three-point loading
m mass of falling sphere
n number of blows needed to fracture specimen
P maximum force carried by specimen in quasi-static three-point loading

Introduction

High-performance mortar (HPM) is a novel composite renowned with its high strength and low permeability. These characteristics make HPM suitable for special structural and defensive purposes, so attempts to improve mechanical properties such as flexural strength, compressive strength and impact resistance are developing quickly (Einsfeld and Velasco, 2006; Sovjak *et al.*, 2013). HPM is brittle in nature, with low flexibility. To overcome these weaknesses, various reinforcements (e.g. steel fibres) have been studied as a way of enhancing its mechanical stability (Marar *et al.*, 2001; Soroushian *et al.*, 1990).

Carbon nanotubes (CNTs) with cylindrical nanostructure exhibit extremely good mechanical, electrical and physical properties. For example, CNTs demonstrate a high strength to weight ratio (100 times greater than that of steel) and outstanding Young's modulus and tensile strength – as high as 1 TPa and 200 GPa respectively (Chaipanich *et al.*, 2010; Li and Chou, 2003). CNTs are classified into single-walled carbon nanotubes (SWCNTs) and multi-walled carbon nanotubes (MWCNTs). SWCNTs are composed of one rolled sheet of graphite with an average diameter around 1 nm, whereas MWCNTs are composed of multiple concentric layers of graphite sheets with average diameter of about 10 nm (Al-Rub *et al.*, 2012; Nochaiya and Chaipanich, 2011).

Because of the abovementioned advantages, CNTs have been used widely to reinforce composite matrices, leading to improvements in the mechanical properties of the polymer–CNT composite (Lau and Hui, 2002).

Chaipanich *et al.* (2010) investigated the compressive strength and microstructure of CNT–fly ash cement composites. They reported that the addition of CNTs increased the compressive strength of the composites and their experimental results confirmed that the interaction between the CNTs and the fly

ash cement matrix was excellent. CNTs can thus act as a filler and improve the microstructure and strength of cement composites.

Gdoutos *et al.* (2010) investigated macroscale and nanoscale mechanical properties in addition to the nanostructure of cement nanocomposites reinforced with different length MWCNTs. Using ultrasonic energy and surfactant for a high dispersion of MWCNTs in water, their results showed that ultrasonic energy increased the dispersion of MWCNTs. Furthermore, an optimum weight ratio of surfactant to CNTs close to 4·0 improved the dispersibility of CNTs in water. Proper dispersion of MWCNTs resulted in improved fracture properties and reinforcement of the cement matrix.

Li *et al.* (2005) investigated the mechanical behaviour and microstructure of cement composites including functionalised MWCNTs. Their results showed that the treated nanotubes improved the flexural strength, compressive strength and failure strain of cement matrix composites.

Musso *et al.* (2009) reported on the influence of CNT structure on the mechanical behaviour of cement composites. Their results showed that the mechanical strength of the cement composites was strongly affected by the defects and chemical properties of the utilised MWCNTs. They also reported that a significant number of defects in the CNT atomic network enhanced the ultimate strength of the nanocomposites.

Marar *et al.* (2001) determined the impact resistance of a high-strength fibre-reinforced concrete composite and found that the application of steel fibres in the concrete improved the impact resistance and compression toughness of the composite.

Sobolkina *et al.* (2012) studied the mechanical properties of cement–MWCNT composites. According to their results, proper dispersion was achieved with a CNT to surfactant ratio of 1·0:1·0 to 1·0:1·5 and a sonication time of 120 min. The cementitious composite modified with CNTs showed a significant increase in compressive strength, but the surfactant decreased the strength due to foam formation during mixing of the cement paste.

Einsfeld and Velasco (2006) reported on the fracture properties of high-performance concrete from 115 three-point bending tests on specimens with different compressive strengths. Their experimental results obtained by the work-of-fracture method revealed that fracture energy increased as the compressive strength of the concrete increased.

Kim *et al.* (2011) studied the influence of macrofibres on the flexural performance of hybrid ultrahigh-performance fibre-reinforced concretes (H-UHPFRCs). They used four types of high-strength steel macrofibres and reported that the H-UHPFRCs showed significantly better flexural performance than UHPFRC reinforced with microfibres.

Although the mechanical properties of cement and concrete reinforced with micro- and macrofibres have been investigated by many researchers, the influence of CNTs on the impact resistance, compressive strength and flexural strength of HPM has not yet been reported. This paper aims to fill that gap.

Materials and methods

Functionalised MWCNTs produced by way of the chemical vapour deposition method were used as reinforcing materials; their specifications are listed in Table 1. The HPM was prepared using Portland cement type II and microsilica with the compositions shown in Table 2. In addition to these materials, silica powder comprising grains of silica of size 0–90 μm was used as filler and silica sand of size 90–500 μm was used as coarse aggregate. In order to reduce the water to cementitious materials ratio, a superplasticiser (SP) based on polycarboxylate ether was also used.

To make the specimens, cement and microsilica were mixed for 2 min to obtain a uniform composition. Silica sand and silica powder were then added to the mixture and mixing was continued for a further 5 min. Functionalised MWCNTs at a dosage of 0·1% weight of cement were dispersed in water and sonicated at room temperature for 5 min in a 750 W ultrasonic processor

Purity: %	>95%
Inner diameter: nm	3–15
Outer diameter: nm	8–15
Length: nm	5×10^4
Specific surface area: mm^2/g	233×10^6
Electrical conductivity: S/mm	1000
Real density: g/mm^3	$2{\cdot}1\times10^3$
Carboxylic groups: %	2·56

Table 1. Specification of the MWCNTs

	Cement	Microsilica
Silicon dioxide (SiO_2): %wt	21·63	93·6
Silicon trioxide (SiO_3): %wt	2·02	0·10
Magnesium oxide (MgO): %wt	2·77	0·97
Calcium oxide (CaO): %wt	63·25	0·49
Iron oxide (Fe_2O_3): %wt	3·45	0·37
Aluminium oxide (Al_2O_3): %wt	2·27	1·32
Chlorine (Cl): %wt	—	0·04
Phosphorus pentoxide (P_2O_5): %wt	—	0·16
Potassium oxide (K_2O): %wt	—	0·01
Carbon (C): %wt	—	0·30
Silicon carbide (SiC): %wt	—	0·50
Sodium oxide (Na_2O): %wt	—	0·31
Tricalcium aluminate (C_3A): %wt	5·48	—

Table 2. Components of cement and microsilica

operated at an amplitude of 50%. The MWCNT suspension was added to the cement mixture and mixed for 2 min. SP was then added to the mixture and mixing was carried out for a further 2 min. The preparation procedure of the control samples was the same as that used for the reinforced HPM (RHPM), but without the addition of MWCNTs. The final mixtures had high viscosity and consistency. The mix designs of the HPM and RHPM are shown in Table 3, where SP/c, CNT/c and w/c are the ratios of SP, CNTs and water to cement respectively. Finally, the mortars were poured into oiled moulds – the mould dimensions were $50 \times 50 \times 50$ mm for compressive strength testing and $300 \times 100 \times 50$ mm for impact resistance and flexural strength tests. Immediately after the pouring step, all the moulds are placed on a vibrating table for 30 s to remove entrapped air. The sample surfaces were smoothed and covered with wet cloth, demoulded after 1 d and maintained in a water bath at 25°C. The compressive strength, impact resistance and flexural strength were measured after 28 d.

Fourier transform infrared (FTIR) measurements (Tensor 70) were conducted to study the functional groups of the outer surface of the MWCNTs. X-ray powder diffraction (XRD), using a PC1800X diffractometer (40 kV/30 mA) with CuKα (0·1542 nm) radiation, was also performed to characterise the phase composition of the MWCNTs. The scanning velocity was 0·02°/s, and the scanned 2θ ranged from 8° to 90°. Scanning electron microscopy (SEM) micrographs were used to investigate the bridge performance of the CNTs; these were obtained using a LEO 450 vp system operating at 30 kV.

The compressive strength of the samples was measured according to ASTM C109/C109M (ASTM, 2013). The cubic specimens were loaded using a hydraulic jack and the time from beginning of loading to fracture was approximately 60 s.

The impact resistance of the samples was measured using the set-up illustrated schematically in Figure 1. To eliminate friction and obtain more accuracy, a powerful electromagnetic that could hold the impact spheres at a defined height (500–5000 mm) was used in this device; a steel sphere of mass 0·92 kg and a falling height $h = 500$ mm were used to strike the specimens. Support for the set-up included a thick plate and two cubic seats with rollers. Specimens were placed on the rollers, which were free to rotate. With the power to the electromagnet turned off, the steel sphere fell. With friction close to zero, the potential energy of the steel sphere is thus completely transferred to the mortar sample.

	Constituent: kg/m^3				w/c	SP/c	CNT/c
	Cement	Microsilica	Filler	Silica sand			
HPM	800	375	300	800	0·3	0·03	—
RHPM	800	375	300	800	0·3	0·03	0·001

Table 3. Mix design of HPM and RHPM

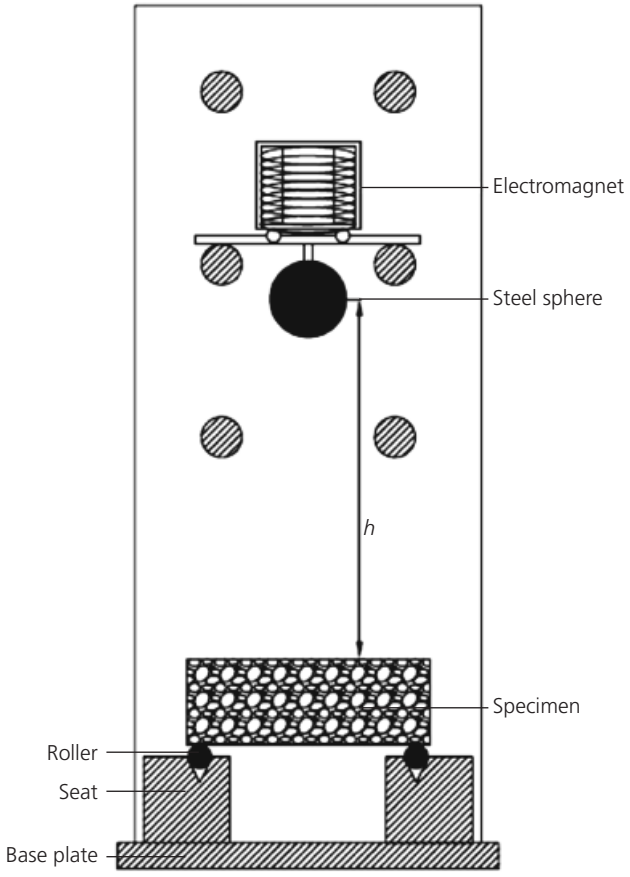

Figure 1. Impact resistance test set-up

Equations 1 and 2 represent the unique impact energy and the total failure energy of samples respectively (Taylor, 2004)

$$1. \quad E = mgh$$

$$2. \quad E_t = nE$$

in which m is the mass of the steel sphere, $\boldsymbol{g}$ is gravitational acceleration, h is the height fall and n is the number of impacts needed until fracture of the sample.

Flexural strength tests on the HPM and RHPM were conducted using quasi-static three-point loading and a hydraulic jack (Figure 2). The set-up comprised two beams, with a separation of 250 mm between their centres, upon which specimens were placed for flexural strength testing. The flexural load was increased at a rate of 2 MPa/min, which is double the loading rate suggested in ASTM C293-08 (ASTM, 2010). After fracture of

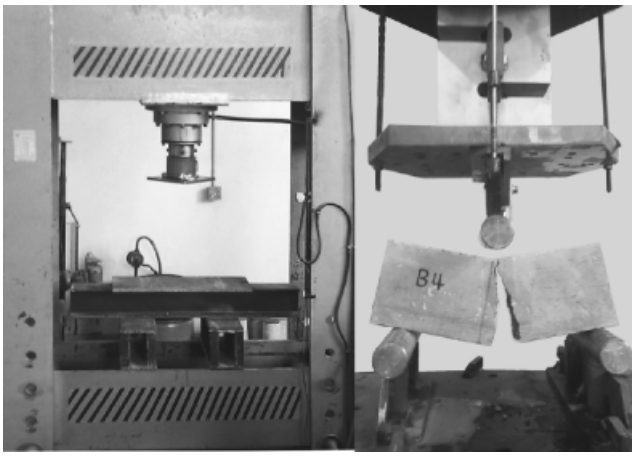

Figure 2. Flexural resistance test set-up

the sample, the modulus of rupture (MoR) can be calculated from Equation 3 in which P is the ultimate load, L is the clear span between the beams (250 mm), d is the specimen depth (100 mm) and b is its width (50 mm)

$$\text{MoR} = \frac{3PL}{2bd^2} \quad (3)$$

Results and discussion

Characterisation of MWCNTs

As noted earlier, FTIR analysis was performed to confirm the presence of functional groups on the outer surface of the MWCNTs. The FTIR spectrum of the functionalised MWCNTs in the range 40–400 mm^{-1} is shown in Figure 3. The absorptions at 173 mm^{-1} and 344 mm^{-1} are attributed to the presence of carboxylic and hydroxyl groups, resulting from oxidation of the MWCNTs. The introduction of these oxygen-containing groups on the outer surface of MWCNTs leads to a high dispersion of the CNTs in a polar solution such as water (Hu *et al.*, 2006). In addition, an absorbance band at 162 mm^{-1} appears in the spectrum, which is attributed to the stretching frequencies of the C=C bonds of the MWCNTs (Kitamura *et al.*, 2011). The absorption peak at 157 mm^{-1} is attributed to the C–C bond stretching vibration of the carbon skeleton of the MWCNTs (Barick and Tripathy, 2011). The peak at 116 mm^{-1} is related to C–O stretching transitions, most likely due to the formation of carboxylic acid groups.

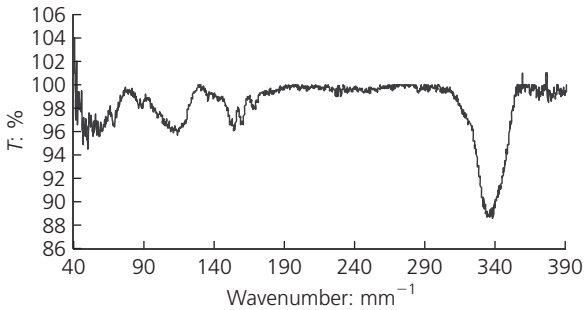

Figure 3. FTIR spectrum of functionalised MWCNTs

Figure 4 shows the XRD pattern of the functionalised MWCNTs. There is a sharp peak at around $2\theta = 26°$ and a broad peak centred at $2\theta = 43°$, corresponding to the (002) and (100) Bragg reflection planes having interlayer spacings of 0·335 nm and 0·203 nm respectively. Bragg's law gives the angles for coherent and incoherent scattering from a crystal lattice. At certain specific wavelengths and incident angles, crystalline solids produce intense peaks of reflected radiation known as Bragg peaks. Incident X-ray radiation produces a Bragg peak if reflections off various planes interfere constructively (Cowley, 1975). The peak at $2\theta = 26{\cdot}603°$ is typical of the (002) diffraction peak of graphite and confirms the presence of CNTs in the samples (Bouazza *et al.*, 2009).

Compressive strength of RHPM

The compressive strengths (average value of three samples) of HPM and RHPM are shown in Figure 5. It is clear that the application of MWCNTs has a significant effect on compressive strength, increasing from 86 MPa for HPM to 108 MPa for

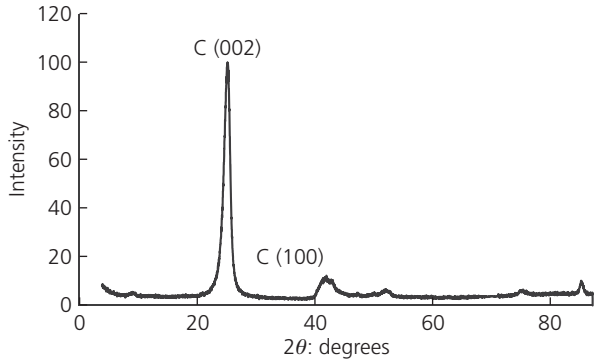

Figure 4. XRD pattern of functionalised MWCNTs

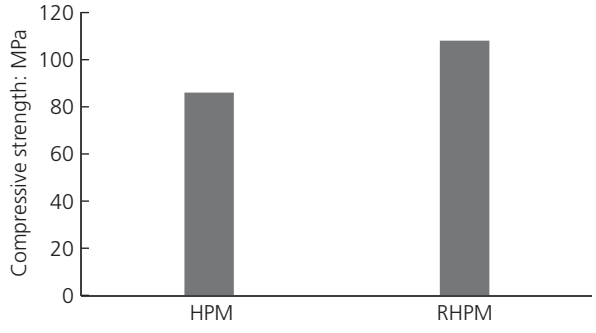

Figure 5. Effect of MWCNT addition on the compressive strength of HPM

RHPM (i.e. an increase of 25·58%). This could be due to modification of the microstructure of the RHPM as CNTs have a bridge coupling effect in the matrix.

Impact resistance of RHPM

The results from the impact resistance tests on HPM and RHPM are listed in Table 4 and the average values of three samples are shown in Figure 6. The effect of MWCNT addition is striking: the impact resistance of the control sample without MWCNTs is 12 J, whereas the impact resistance for RHPM containing 0·1 %wt MWCNTs is 180·5 J (more than 14 times the control sample). The increase in impact resistance of RHPM is due to the unique mechanical properties of MWCNTs, with MWCNTs filling small pores in the mortar (Vikas *et al.*, 2008), resulting in a denser mortar with reduced permeability. Interfacial interactions also exist between hydration products and the MWCNTs, which also increases the impact resistance of RHPM (Chaipanich *et al.*, 2010; Nochaiya and Chaipanich, 2011).

From another point of view, CNTs increase the hardness of calcium silicate hydrate crystals. Calcium silicate hydrate is mainly responsible for the hardening process and the ultimate strength of mortar, increasing its hardness and rigidity. RHPMs are thus more resistant to impact loading (Gdoutos *et al.*, 2010).

Sample	Number of blows, *N*	Sphere mass: kg	Fall height: mm	Unique impact energy: J	Failure energy: J
HPM					
H1	2	0·920	500	4·51	9·0
H2	3	0·920	500	4·51	13·5
H3	3	0·920	500	4·51	13·5
RHPM					
RH1	40	0·920	500	4·51	180·5
RH2	40	0·920	500	4·51	180·5
RH3	40	0·920	500	4·51	180·5

Table 4. Impact resistance of specimens

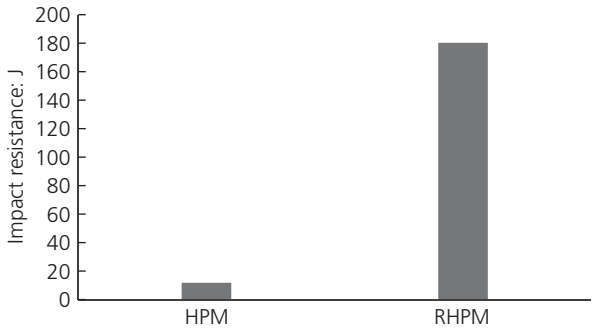

Figure 6. Effect of MWCNTs on the impact resistance of HPM

Flexural strength of RHPM

Figure 7 shows that there is no major difference between the flexural strengths of the HPM and RHPM, but the addition of 0·1 %wt MWCNTs did increase the flexural strength of the mortar slightly from 9·35 MPa to 9·55 MPa (an increase of 2%). The ineffectiveness of CNTs in increasing the flexural strength of HPM is due to their micrometric length and the mechanism of action of quasi-static loading. Macrofibres have a bridge effect in mortar structures: they are gradually pulled out from the mortar matrix upon increasing crack widths and therefore improve the ductility and flexural resistance of HPMs (Marar *et al.*, 2001). Quasi-static loading causes a large displacement and extreme force in the centre of prismatic specimens over a short period of time. CNTs are therefore pulled out quickly during quasi-static three-point bending loads and do not perform a proper bridge action. The large difference between sample size and dimensions of the nanotubes also renders nanotubes ineffective in quasi-static bending. Sobolkina *et al.* (2012) reported similar results.

Microstructural analysis

Microstructural analysis was performed to explore the effects of MWCNTs on HPM microstructure. Figure 8 is a typical SEM image of HPM, showing obvious microcracks that can be related to the absence of a bridging agent in the mortar. The images of

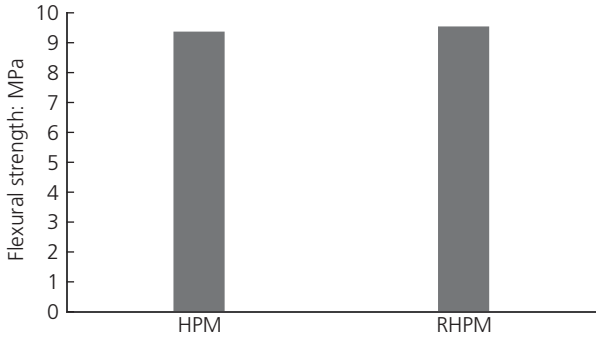

Figure 7. Effect of MWCNTs on the flexural strength of HPM

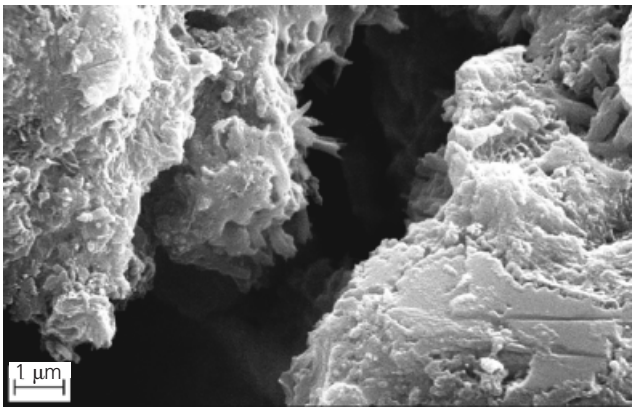

Figure 8. SEM image of HPM control specimen

the HPM reinforced with 0·1 %wt MWCNTs (Figure 9) reveal that the functionalised MWCNTs were dispersed uniformly in the paste and there was no obvious aggregation of MWCNTs. It is also clear that the MWCNTs act as bridging agents to limit the propagation of cracks and densify the HPM. In fact, the observed breakage of the RHPM implies good bonding between the MWCNT surfaces and the components of the HPM. This is related to the embedment of the MWCNTs into the hydration products of HPM, which is consistent with the results obtained by Chaipanich *et al.* (2010).

Conclusions

The effects of functionalised MWCNTs on the mechanical properties of HPM were studied. The experimental results show that the influence of MWCNTs on HPM is affected by the type of loading and test conditions – the compressive strength and impact resistance of RHPM were respectively 25·58% and 1400% higher than the values obtained for the control sample, but the flexural strength increase due to the addition of MWCNTs in quasi-static three-point loading was just 2%.

The dramatic effect of MWCNTs on the impact resistance of HPM and its significant effect on compressive strength are due to the structure of the MWCNTs, their bridging action in the mortar matrix and their effect on improving the hardness of calcium silicate hydrate crystals, all causing increased rigidity and strength of the RHPM. However, in quasi-static three-point loading, MWCNTs are affected by the high force rate and are pulled out from the HPM matrix very quickly, therefore losing their bridging effect and rendering them ineffective at significantly improving flexural strength.

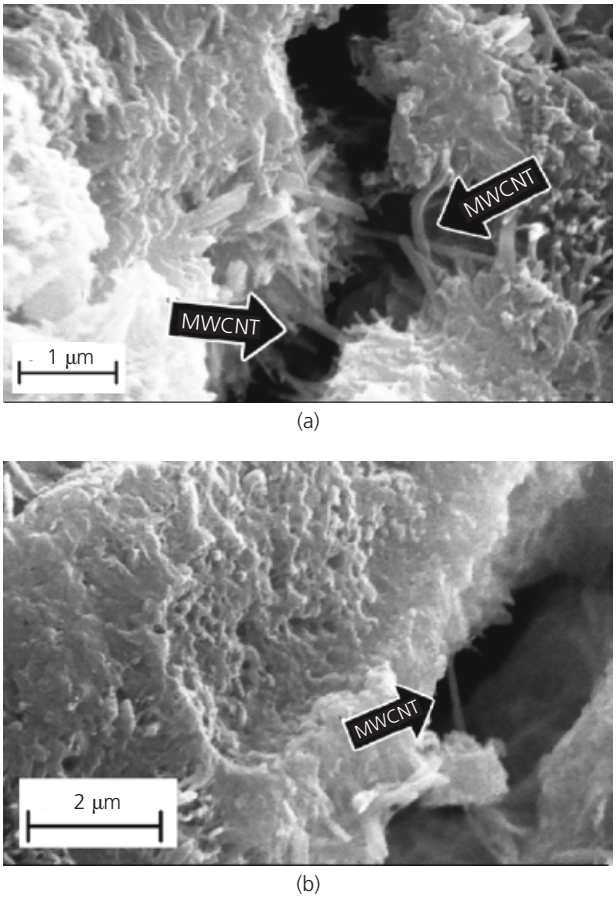

Figure 9. SEM images of HPM reinforced with 0·1 %wt MWCNTs

Supplementary tests in this study (XRD and FTIR analysis) showed that the purity of the used CNTs was about 98% and oxygen-containing groups such as hydroxyl and carboxylic groups were present on their surfaces. Furthermore, SEM images revealed that MWCNTs can act as bridging agents and can limit cracking in HPM microstructures.

This work has shown that the application of a small amount of MWCNTs has a significant effect on the properties of HPM. Therefore, despite their high cost, these materials are useful for enhancing the mechanical properties of HPM.

REFERENCES

Al-Rub RKA, Ashour AI and Tyson BM (2012) On the aspect ratio effect of multi-walled carbon nanotube reinforcements on the mechanical properties of cementitious nanocomposites. *Construction and Building Materials* **35**: 647–655.

ASTM (2010) ASTM C293-08: Standard test method for flexural strength of concrete (using simple beam with center-point loading). ASTM International, West Conshohocken, PA, USA.

ASTM (2013) ASTM C109/C109M: Standard test method for compressive strength of hydraulic cement mortars (using 2 in or [50 mm] cube specimens). ASTM International, West Conshohocken, PA, USA.

Barick AK and Tripathy DK (2011) Preparation, characterization and properties of acid functionalized multi-walled carbon nanotube reinforced thermoplastic polyurethane nanocomposites. *Materials Science and Engineering B* **176(18)**: 1435–1447.

Bouazza N, Ouzzine M, Lillo-Ródenas MA, Eder D and Linares-Solano A (2009) TiO_2 nanotubes and CnT-TiO_2 hybrid materials for the photocatalytic oxidation of propene at low concentration *Applied Catalysis B Envrionmental* **92(3–4)**: 377–383.

Chaipanich A, Nochaiya T, Wongkeo W *et al.* (2010) Compressive strength and microstructure of carbon nanotubes–fly ash cement composites. *Materials Science and Engineering A* **527(4–5)**: 1063–1067.

Cowley JM (1975) *Diffraction Physics*, 3rd edn. Elsevier, Amsterdam, the Netherlands.

Einsfeld RA and Velasco MSL (2006) Fracture parameters for high-performance concrete. *Cement and Concrete Research* **36(3)**: 576–583.

Gdoutos MSK, Metaxa ZS and Shah SP (2010) Highly dispersed carbon nanotube reinforced cement based materials. *Cement and Concrete Research* **40(7)**: 1052–1059.

Hu CY, Li FY, Hua L *et al.* (2006) A study concerning the pretreatment of CNTs and its influence on the performance of NiB/CNTs amorphous catalyst. *Journal of the Serbian Chemical Society* **71(11)**: 1153–1160.

Kim DJ, Park SH, Ryu GS *et al.* (2011) Comparative flexural behavior of hybrid ultra high performance fiber reinforced concrete with different macro fibers. *Construction and Building Materials* **25(11)**: 4144–4155.

Kitamura H, Sekido M, Takeuchi H *et al.* (2011) Method for surface functionalization of single-walled carbon nanotubes with fuming nitric acid. *Carbon* **49(12)**: 3851–3856.

Lau KT and Hui D (2002) The revolutionary creation of new advanced materials–carbon nanotube composites. *Composites Part B: Engineering* **33(4)**: 263–277.

Li C and Chou T (2003) Elastic moduli of multi-walled carbon nanotubes and the effect of van der Waals forces. *Composite Science and Technology* **63(11)**: 1517–1524.

Li GY, Wang PM and Zhao X (2005) Mechanical behavior and microstructure of cement composites incorporating surface-treated multi-walled carbon nanotubes. *Carbon* **43(6)**: 1239–1245.

Marar K, Eren O and Celik T (2001) Relationship between impact energy and compression toughness energy of high-strength fiber-reinforced concrete. *Materials Letters* **47(4–5)**: 297–304.

Musso S, Tulliani JM, Ferro G *et al.* (2009) Influence of carbon nanotubes structure on the mechanical behavior of cement composites. *Composites Science and Technology* **69(11)**: 1985–1990.

Nochaiya T and Chaipanich A (2011) Behavior of multi-walled carbon nanotubes on the porosity and microstructure of cement-based materials. *Applied Surface Science* **257(6)**: 1941–1945.

Sobolkina A, Mechtcherine V, Khavrus V *et al.* (2012) Dispersion of carbon nanotubes and its influence on the mechanical properties of the cement matrix. *Cement and Concrete Composites* **34(10)**: 1104–1113.

Soroushian P, Bayasi Z and Khan A (1990) *Thin Section Fiber Reinforced Concrete and Ferrocement*. American Concrete Institute, Hacienda Heights, CA, USA.

Sovjak R, Vavrivik T, Maca P *et al.* (2013) Experimental investigation of ultra-high performance fiber reinforced concrete slabs subjected to deformable projectile impact. *Procedia Engineering* **65**: 120–125.

Taylor JR (2004) *Classical Mechanics*. Edward brothers, Ann Arbor, MI, USA.

Vikas K, Bakshi BR and Lee LJ (2008) Carbon nanofiber production: life cycle energy consumption and environmental impact. *Journal of Industrial Ecology* **12(3)**: 394–410.